

## Effectiveness of Cobalt-Doped Biochar Derived from Durian Shell for Degradation of Rhodamine B

Anh Mai Hoang Trinh<sup>1</sup>, Thinh Phu Le<sup>1</sup>, Khoi Anh Tran<sup>2</sup>, Nga Hoang Nguyen Do<sup>1</sup>, Kien Anh Le<sup>2</sup>, Viet Tan Tran<sup>1</sup>, and Phung Kim Le<sup>3\*</sup>

<sup>1</sup>Faculty of Chemical Engineering, Ho Chi Minh City University of Technology (HCMUT), 268 Ly Thuong Kiet Street, District 10, Ho Chi Minh City 700000, Vietnam

<sup>2</sup>Institute for Tropical Technology and Environmental Protection, 57A Truong Quoc Dung Street, Phu Nhuan District, Ho Chi Minh City 700000, Vietnam

<sup>3</sup>CIRTECH Institute, HUTECH University, 475A Dien Bien Phu Street, Ho Chi Minh City 700000, Vietnam

\* **Corresponding author:**

email: ltk.phung@hutech.edu.vn

Received: August 19, 2024

Accepted: November 25, 2024

DOI: 10.22146/ijc.99181

**Abstract:** The global discharge of dye-contaminated effluent into the environment has garnered considerable public attention, and removing the organic pollutants from wastewater is of great importance. Durian shell, a major by-product of Asia countries, is one of the primary causes of environmental issues. To address these current issues, the development of efficient and eco-friendly biomass-derived catalysts that activate advanced oxidation processes (AOP) stands out as a crucial technology for treating organic pollutants in water. In this study, cobalt-doped biochar composites (CoC-n) were synthesized using solvothermal and calcination techniques, with durian shell biomass serving as the precursor material. The obtained CoC-n treated under various calcination temperatures analyzed via SEM, EDS, XRD, and FTIR techniques, which were used for efficient peroxymonosulfate (PMS) activation for up to 92% and 58.98–74.30% RhB (25 and 75 mg/L, respectively) degradation in 30 min. The quenching test performed on the CoC-350/PMS system revealed that RhB degradation involves sulfate ( $\text{SO}_4^{\cdot-}$ ), hydroxyl ( $\text{OH}^{\cdot}$ ), and singlet oxygen ( $^1\text{O}_2$ ) in RhB degradation, with  $\text{SO}_4^{\cdot-}$  and  $^1\text{O}_2$  being the primary components. The cobalt-doped biochar from durian shells is considered a novel and promising candidate for the eradication of dye-contaminated effluent applications.

**Keywords:** durian shell; AOP; rhodamine B; cobalt-doped biochar

### ■ INTRODUCTION

Rapid industrialization and civilization have led to the widespread dissemination and accumulation of various toxic organic pollutants, which are challenging to treat by conventional methods. Approximately 60,000 tons of dyes are released annually into the environment worldwide, with azo dyes constituting 80% of these chemicals [1]. One such dye, Rhodamine B (RhB), a reddish violet-colored powdered substance, has gained extensive industrial use due to its remarkable characteristics, including high water solubility, incredible brightness, and good stability [2]. Despite its usefulness, RhB dyes have been associated with significant harmful

effects on both human well-being and the environment. They exhibit neurotoxic and carcinogenic properties, impede organismal development, and pose a general hazard to ecosystems. In addition, RhB can irritate as exposed to humans' eyes, skin, and respiratory tract [1,3]. To address this issue, various methods have been developed to remove RhB dyes from wastewater, including membrane separation, adsorption, flocculation, extraction, biodegradation, and advanced oxidation processes (AOPs) [2,4].

Among these methods, AOPs have gained considerable interest as efficient methods for directly remediating contaminants and converting them into decomposable low-molecular-weight organic matter

through induced oxidation/reduction reactions. Because of their adaptability and environmental friendliness, sulfate radical-based AOPs, which entail the formation of sulfate and hydroxyl radicals, have drawn interest recently. This sulfate radical-based AOPs possess superior properties, such as a higher oxidizing potential ranging from 2.6 to 3.1 V, wider pH tolerance of 2–9, and a longer half-life of 30–40  $\mu$ s, making them more viable alternatives to typical hydroxyl radical-based AOPs [5]. In the scope of environmental-related applications, peroxydisulfate (PDS) has been extensively utilized for its enhanced reactivity, which is a result of its large O–O bond length and asymmetric structure [5-6]. In general, physical and chemical techniques can be used to activate PDS in order to produce sulfate radicals. The most commonly used activation methods include the use of metal or non-metal catalysts, heat, ultrasound, electrochemistry, alkali, UV or visible light, microwave, and photocatalytic activation [5].

In particular, heterogeneous systems employing metal ion catalysts have been extensively studied due to their sizeable interactive surface area, stable structure, and convenient recovery [7]. Cobalt has been demonstrated to outperform other metal catalysts, serving as a highly effective heterogeneous catalyst for the activation of PDS during catalytic reactions. The reactive oxygen species (ROS), such as singlet oxygen ( $^1\text{O}_2$ ), hydroxyl ( $\text{OH}^\bullet$ ), and sulfate ( $\text{SO}_4^{\bullet-}$ ), can be generated directly from the activation of PDS by heterogeneous catalysts [8]. These species serve as potential oxidizing agents capable of decomposing organic pollutants into low-toxicity intermediates or even mineralized products of  $\text{H}_2\text{O}$  and  $\text{CO}_2$ . However, the leaching of metal ions poses a potential risk to human well-being and environmental security, and the difficulty in reclamation has hindered the widespread utilization of metal-based catalysts [7]. Cobalt-based heterogeneous catalysts, such as  $\text{CoFe}_2\text{O}_4$ -EG,  $\text{CoFeNi}$ -LDH,  $\text{Co}_3\text{O}_4$ -palygorskite, and  $\text{LSCO}_5/\text{CGCNx}$ , have demonstrated effectiveness in activating PDS for organic degradation; nonetheless, they exhibit varying levels of cobalt leaching, reported to range from 0.13 to 0.90 mg/L [9-12]. The release of cobalt ions can lead to the contamination of aquatic ecosystems and soils, with the

potential for bioaccumulation in the human food chain [13]. Furthermore, cobalt leaching adversely affects the catalytic performance of these materials, and the challenges associated with reclaiming used catalysts complicate efforts to mitigate their environmental impact [7,14]. To address these limitations, various approaches have been explored, including modification, doping, coating, the use of hybrid materials, and synthesis on carbon substrates.

Biochar, a carbon-rich material derived from biomass, exhibits considerable potential in environmental remediation and serves as an ideal carrier for catalysts comprised of metals. Various thermochemical processes can be utilized to produce biochar from biomass, including hydrothermal carbonization and gasification conducted in an oxygen-limited environment [15-16]. This production is due to its advantageous physicochemical properties, such as high specific surface area, a highly porous nature, and plenty of reactive functional groups [17]. Biochar-supported material exhibits not only significant potential for activating PDS but also a wide variety of applications as environmentally friendly carbon materials. The use of transition metal-doped biochar, primarily cobalt, as a catalyst for PDS activation in organic solvent treatment has emerged as a significant area of research in water remediation. Zang et al. [18] used iron-doped biochar, derived from waste sludge, as a catalyst to activate PDS for the degradation of RhB. The catalyst was prepared using the hydrothermal carbonization method. Systems exhibited exceptional activity and durability, achieving more than a twofold increase in effectiveness and nearly complete degradation of 50 mg/L RhB in 10 min. In 2022, Liu et al. [19] employed the via incipient wetness impregnation to load cobalt nanoparticles into a biomass template derived from rose petals, followed by one-step pyrolysis at 800  $^\circ\text{C}$ , resulting in a highly efficient PDS-activating catalyst for levofloxacin degradation, with complete degradation of a 10 mg/L solution within 10 min, primarily facilitated by  $^1\text{O}_2$  generation and electron transfer processes. Similarly, in 2023, Wang et al. [20] synthesized iron and cobalt co-doped biochar from

coconut shell as a PMS-activating catalyst for sulfamethoxazole degradation, achieved through impregnation method and pyrolysis at 800 °C, completely degrading 0.04 mM sulfamethoxazole within 10 min. In catalytic systems, biochar serves as a support material that effectively anchors the metal particles, thereby ensuring the efficiency and stability of the catalysts.

Durian, known as the “king of fruits”, is one of the most prolific fruits in Southeast Asia due to its unique flavor and aroma. According to the Food and Agriculture Organization (FAO), global durian production reaches more than 3 million tons annually, with the region contributing to more than 97% of the total output [21]. While this presents significant economic opportunities for the countries involved, the tremendous waste generated from durian residues, including shells and seeds, poses massive environmental challenges. A promising strategy to mitigate this issue consists of the conversion of durian shells into a source of renewable carbon materials. These materials, characterized by a microporous structure and large surface area, are valuable for various applications [22]. The production of biochar from durian shells yields economic benefits and results in a material with a complex porous structure and a plethora of functional groups, enhancing its capacity to support nanoparticle loading [23]. However, the presence of unexpected components like pectin, lignin, and waxes within the structure of durian shells exerted an influence on the structure of materials [24]. While acid pretreatment is widely recognized as an effective approach to eliminating unexpected components from biomass, recent studies have suggested that char derived from hydrothermal pretreatment may serve as a superior precursor for enhancing porosity in the material [2,25-26].

Herein, cobalt-doped biochar composites (CoC-n) from durian shells were effectively created using an economical and environmentally beneficial method. The fabrication involved hydrothermal pretreatment, metal doping via solvothermal treatment, and calcination steps. The as-prepared CoC-n catalyst was subsequently employed for PMS activation in the degradation process of RhB dye. The influence of calcination temperature on

the physicochemical properties and capability of CoC-n catalyst for RhB was comprehensively investigated through advanced characterization techniques. Additionally, a competitive quenching test was conducted to identify the specific ROS responsible for the observed RhB degradation.

## ■ EXPERIMENTAL SECTION

### Materials

The durian shell was collected from a local fruit market in Ho Chi Minh City, Vietnam. Urea ((NH<sub>2</sub>)<sub>2</sub>CO), cobalt nitrate hexahydrate (Co(NO<sub>3</sub>)<sub>2</sub>·6H<sub>2</sub>O), tert-butyl alcohol (TBA, 99.5%), and ethanol (EtOH, 99.8%) were purchased from Xilong Scientific Co. PMS was purchased from Damas-beta. RhB was obtained from Himedia. Furfuryl alcohol (FFA, 99.5%) was purchased from Shanghai Macklin Biochemical Co., Ltd. All chemicals used in this study were received without further purification unless otherwise stated. Moreover, reverse osmosis (RO) water was employed to prepare all reagents.

### Instrumentation

Various characterization techniques were employed to examine the compounds after calcination treatment. Scanning electron microscopy (SEM) equipped with an energy-dispersive X-ray spectroscopy (EDS) detector taken on a Tescan Mira enables the observation of sample surface morphology and the analysis of elemental composition in the samples. Prior to imaging, a thin layer of Pt was sputtered onto the specimens to enhance the resolution of the captured images. Nitrogen physisorption measurements were conducted on samples pretreated by heating under vacuum at 150 °C for 6 h, using a Micromeritics ASAP 2020 to assess surface behavior at 77 K with high-purity nitrogen gas. Powder X-ray diffraction (XRD) analysis was conducted using an Aeris Benchtop XRD System with Cu-K $\alpha$  radiation ( $\lambda = 0.1542$  nm). This technique provided insights into the crystal phases present in the materials and allowed for the determination of sample purity. Fourier transform-infrared spectroscopy (FTIR) measurements were performed using a Bruker ALPHA

II instrument. This technique focused on investigating the surface functional groups within the samples. The FTIR analysis covered a range of  $500\text{--}4000\text{ cm}^{-1}$  with a resolution of  $4\text{ cm}^{-1}$ .

## Procedure

### Hydrothermal pretreatment of durian shell

To conduct hydrothermal pretreatment on durian shell, the following procedures were implemented. Fresh durian shells were recovered within one day of deshelling, and the white endocarp layer was separated. The endocarp layer was then thoroughly washed to eliminate any remaining durian aril and cut into small pieces measuring approximately  $2\text{ cm}^3$ . These endocarp pieces were subjected to hydrothermal pretreatment by being placed in a Teflon-lined stainless-steel autoclave with RO water. The volume of the mixture was adjusted to constitute 60% of the total autoclave volume. The autoclave was heated to  $180\text{ }^\circ\text{C}$  and maintained at this temperature for 5 h under self-generated pressure within a closed system. After the completion of the hydrothermal treatment, the durian shells were immersed in a solution consisting of ethanol and water in a 1:1 ratio (v/v) for 48 h. During this time, the solution was refreshed every 6 h to ensure the removal of soluble impurities. Subsequently, the treated shells, named DA, were frozen overnight and subjected to freeze-drying under vacuum conditions for 48 h.

### Catalyst preparation

For the preparation of the cobalt-doped biochar catalyst, a combination of solvothermal and calcination methods was used. The procedure began with immersing

1.0 g of DA into a solution containing  $\text{Co}(\text{NO}_3)_2 \cdot 6\text{H}_2\text{O}$  (0.582 g), urea (1.0 g), and 50.0 mL ethanol. This mixture was allowed to react for 2 h at a temperature of  $30\text{ }^\circ\text{C}$ , followed by the solvothermal process at  $120\text{ }^\circ\text{C}$  for 10 h. The resulting product was then dried at  $50\text{ }^\circ\text{C}$  for 12 h to ensure complete removal of the liquid remains, referred to as CoDA. Next, the dried CoDA product was placed in a muffle furnace, and a temperature ramp was applied from  $300$  to  $500\text{ }^\circ\text{C}$  at a rate of  $5\text{ }^\circ\text{C}/\text{min}$  under limited oxygen conditions. The material was maintained at the final temperature for 2 h. The as-obtained black catalyst was finely ground using a porcelain mortar and pestle and subsequently stored in an oven, dried at  $50\text{ }^\circ\text{C}$  overnight for further experimentation. The catalysts prepared under different conditions were named CoC-n, where n represents the calcination temperature of the CoDA precursor used in the process. Fig. 1 shows the synthesis process of CoDA.

### Dye degradation test

In a degradation experiment, 200 mL of RhB solution (25 and 75 mg/L) was placed in a beaker with 0.06 g of catalyst CoC-n (0.30 g/L) added and stirred mechanically at 100 rpm. To achieve full contact between the RhB solution and the CoC-n catalyst/PMS system, PMS (0.20 g/L) was added to the solution, and the reaction was started by stirring continuously. At specific time intervals, a measured volume of  $400\text{ }\mu\text{L}$  solution was extracted using a micropipette, and the UV-vis absorbance of the RhB solution was measured. The experiment was repeated three times for each material. RhB concentration was determined using a UV-vis

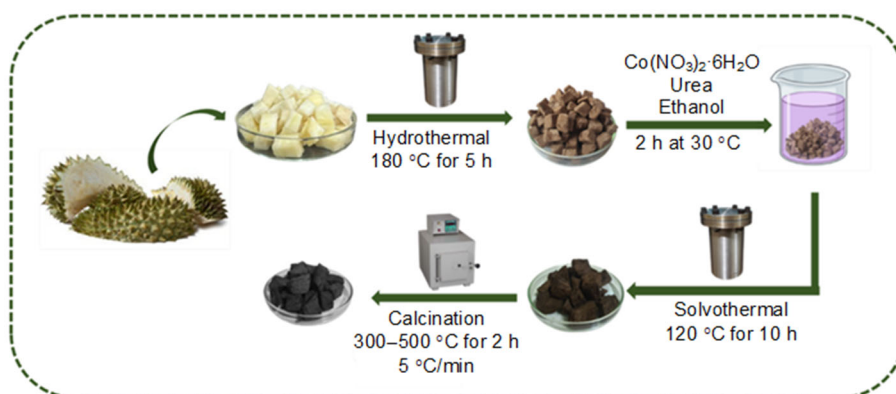


Fig 1. Schematics illustrating the synthesis process of CoC-n catalyst

spectrophotometer (UV-vis Lavionbon Model X7000) at  $\lambda_{\max}$  of 554 nm). An external standard curve was established by correlating the concentrations of standard solutions with their corresponding absorbance values. To calculate the removal efficiency (H%) of the prepared CoC-n catalyst, the Eq. (1) was employed;

$$H = \frac{C_i - C_t}{C_i} \times 100\% \quad (1)$$

where  $C_i$  represents the inlet concentration of RhB solution (mg/L), and  $C_t$  is the concentration of RhB solution (mg/L) at a given time  $t$ .

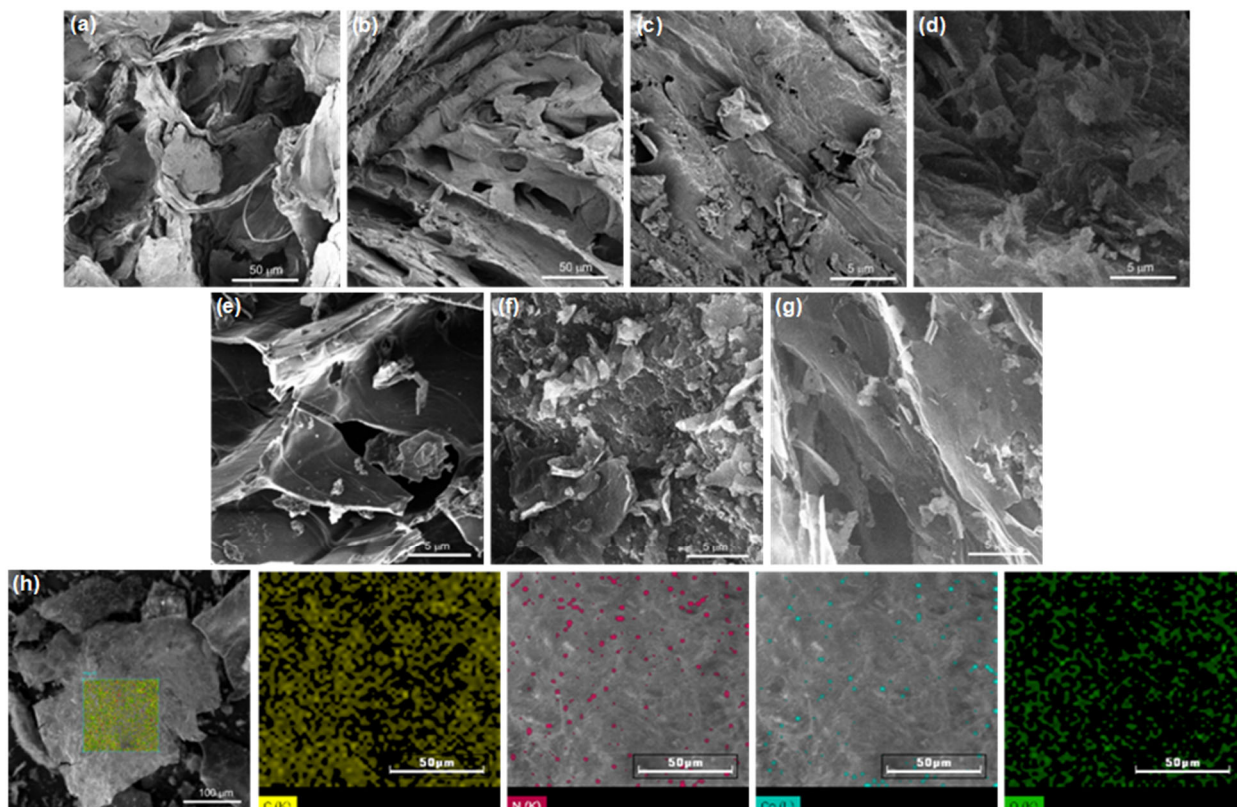
## RESULTS AND DISCUSSION

### CoC-n Material Characterization

The SEM images of the DA, CoDA, and CoC-350 (Fig. 2(a-g)) show the morphological structure of DA, CoDA, and CoC-n. The calcination from 350 to 500 °C led to the development of honeycomb-like porous carbon structures with defined pores. In contrast, the CoC-300 material exhibited a less cracked surface compared to

others despite undergoing the grinding step. Nitrogen adsorption-desorption isotherms, as shown in Fig. 3, revealed that the CoC-350 catalyst displayed a significantly larger BET surface area of 33.23 m<sup>2</sup>/g compared to 4.01 m<sup>2</sup>/g for the CoDA sample. This increased surface area can facilitate better dispersion of the catalyst particles, potentially preventing agglomeration and providing more active sites for catalytic reactions, which may contribute to enhanced catalytic activity.

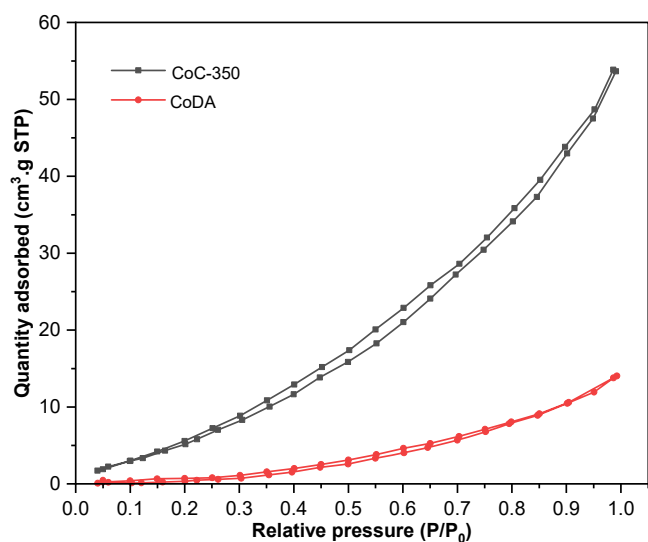
Fig. 2(h) presents the EDS mapping of the CoC-350 composite surface. The mapping reveals a uniform distribution of carbon (C) and oxygen (O) elements across the surface, while nitrogen (N) and cobalt (Co) elements are sparsely detected. Additionally, Table 1 displays the outcomes of the EDS analysis performed on CoDA and CoC-n materials, with measurements carried out at three distinct locations for each sample. The EDX results revealed the presence of C, N, O, and Co elements in all samples. Compared to the theoretical cobalt content



**Fig 2.** Morphologies of (a) DA, (b) CoDA, (c) CoC-300, (d) CoC-350, (e) CoC-400, (f) CoC-450, (g) CoC-500, and (h) elemental mapping images of C, N, O, Co in CoC-350

**Table 1.** Element composition of CoC-n composites via EDS analysis

Sample	Weight (%)			
	C	N	O	Co
CoDA	48.37 ± 1.98	20.97 ± 2.74	22.54 ± 1.41	8.12 ± 1.23
CoC-300	48.08 ± 0.84	17.57 ± 0.80	19.38 ± 0.57	14.97 ± 0.27
CoC-350	57.48 ± 2.03	14.85 ± 0.80	19.11 ± 1.67	8.56 ± 0.69
CoC-400	63.08 ± 1.60	9.99 ± 0.06	19.25 ± 0.71	7.31 ± 1.22
CoC-450	50.82 ± 0.48	11.74 ± 0.72	22.30 ± 0.25	15.13 ± 0.22
CoC-500	63.08 ± 0.67	11.31 ± 0.72	16.85 ± 0.48	8.76 ± 1.04

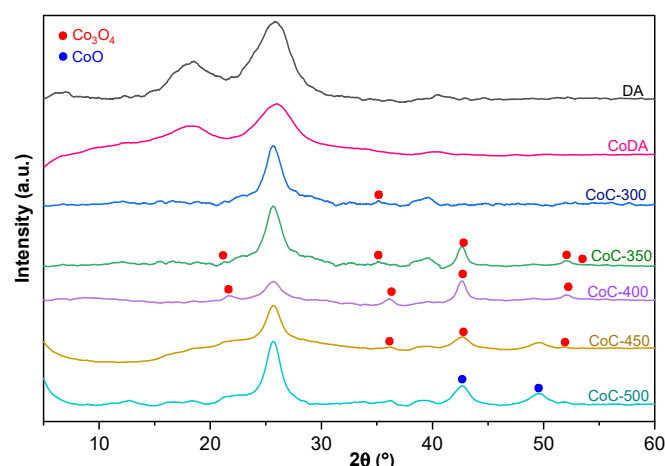
**Fig 3.** Nitrogen adsorption-desorption isotherms of CoDA and CoC-350

of 7.65 wt.%, the cobalt content observed via EDS analysis in the resultant CoC-n catalysts ranged from 8.56 to 15.13 wt.%. This variation signifies heterogeneous cobalt distribution within the material, as EDS measures specific locations and is sensitive to surface composition [27].

According to the XRD patterns depicted in Fig. 4, the presence of the (101) and (200) reflections around 16° and 25° in the DA and CoDA samples indicate the partial charring of the original cellulosic structure [28]. After calcination, disordered graphitic (002) and (100) planes were found between 20–30° and 43° as a result of the predominant carbonaceous structure present in the biochar [28]. Additionally, characteristic peaks at 21.87, 36.08, 42.59, and 51.95° corresponded to the (111), (022), (131), and (040) planes, respectively, compatible with the cubic spinel-phase structure of Co<sub>3</sub>O<sub>4</sub> [29]. However, increasing the calcination temperature to 500 °C led to the

formation of cobalt oxide (CoO), with peaks at 42.62° and 49.63° corresponding to the (111) and (020) planes, respectively [30]. This phenomenon was consistent with previous studies showing that Co<sub>3</sub>O<sub>4</sub> typically forms at 300–450 °C [31–32]. Notably, Co<sub>3</sub>O<sub>4</sub> is more effective than crystalline CoO in activating PMS [33]. The absence of the characteristic peak of cobalt oxide in the CoDA sample could be due to the existence of another form of cobalt.

The results of the FTIR analysis conducted on DA, CoDA, and CoC-n samples are illustrated in Fig. 5. The FTIR spectra of DA revealed numerous distinct peaks characteristic of carbon-based compounds. A broad peak observed at approximately 3360 cm<sup>-1</sup> belonged to the O–H stretching vibration of adsorbed water. In contrast, two adjacent peaks at 2921 and 2848 cm<sup>-1</sup> were assigned to asymmetric and symmetric vibrations of C–H, respectively [34–35]. Peaks at 1611, 1029, and 902 cm<sup>-1</sup>, respectively, were associated with the stretching vibration of the C=C bond, the stretching of

**Fig 4.** XRD patterns of DA, CoDA, and CoC-n

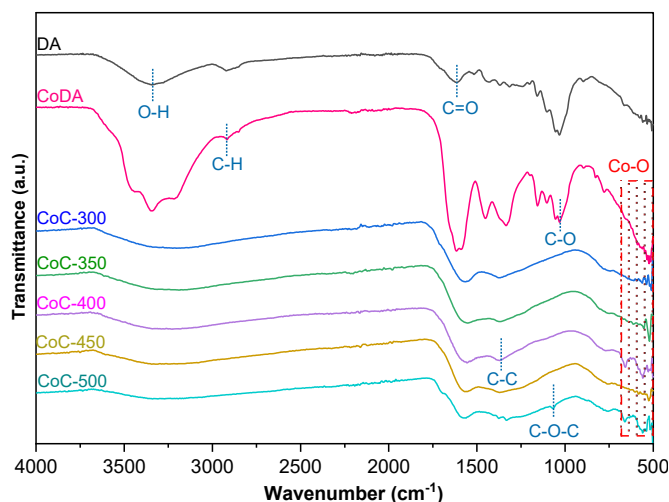


Fig 5. FTIR spectra of DA, CoDA, and CoC-n

the C–O bond, and the bending of the O–H bond [36–37]. In the CoDA spectra, the intensity of the existence peaks notably increased, indicating the presence of numerous oxygen functional groups. Furthermore, the peak intensities at 3360 and 1029  $\text{cm}^{-1}$  significantly decreased, indicating the successful reduction of hydroxyl and epoxide groups in CoC-n following the calcination process. In CoC samples, the characteristic bands originating from the stretching vibrations of the metal–oxygen bonds, namely 567 and 662  $\text{cm}^{-1}$ , were observed, suggesting the presence of  $\text{Co}_3\text{O}_4$  [38]. To be more precise, the  $\text{OB}_3$  vibration in the spinel lattice was linked to the first band at 567  $\text{cm}^{-1}$ , while the  $\text{ABO}_3$  vibration was linked to the second band at 662  $\text{cm}^{-1}$  (where A represents the  $\text{Co}^{2+}$  in a tetrahedral hole and B represents the  $\text{Co}^{3+}$  in an octahedral hole) [39–40].

### Catalytic Performance of the Synthesized CoC-n Samples in PMS Activation

Fig. 6 presents the impact of various systems on the elimination of RhB dye. The application of CoC-350 in isolation demonstrated minimal effectiveness in RhB removal, achieving only 7.40% adsorption within a 30-min interval, primarily due to the predominant adsorption mechanism. In contrast, the use of PMS alone resulted in approximately 15.20% elimination of RhB dye, which could be attributed to its intrinsically low oxidation capacity. However, the combined application of PMS and CoC-350 catalyst significantly increased RhB degradation,

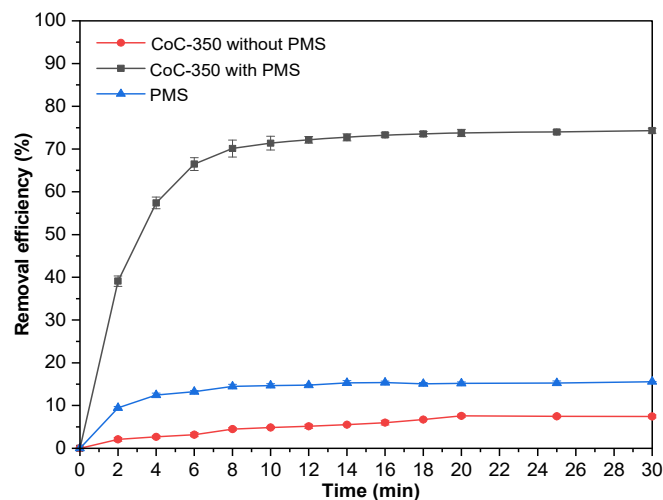


Fig 6. Effect of different systems on RhB degradation

yielding elimination rates that surpassed those of PMS and the catalyst used independently by over five and ten times, respectively. These results underscore the existence of a synergistic interaction between PMS and the CoC-350 catalyst, thereby facilitating an enhanced removal of RhB dye.

Fig. 7 shows the catalytic properties of CoC-n catalysts synthesized at different calcination temperatures. When tested with a 25 mg/L RhB solution, all catalysts demonstrated remarkable efficacy in RhB treatment. CoC-350 and CoC-400 achieved over 90% RhB degradation within a mere 8 min. Moreover, all samples achieved RhB degradation rates exceeding 90% after 10 min. However, as RhB concentration increased, the degradation efficiency of the catalysts declined. Nevertheless, the catalyst still exhibited effective performance, with degradation efficiencies ranging from 58.98 to 74.30%. Notably, CoC-350 displayed the highest degradation efficiency among the tested catalysts, achieving 92.72 and 74.30% within 30 min for 25 ppm and 75 mg/L RhB solutions, respectively.

Furthermore, Table 2 presents a comparative analysis of the catalytic efficacy of various biochar-supported catalysts in activating PMS for the degradation of RhB. Notably, CoC-n achieves exceeding 92.00% degradation efficiency at a dosage of 0.3 g/L within 30 min, positioning it competitively against other biochar-supported catalysts. Additionally, the CoC-n catalyst facilitates the generation of a diverse ROS,

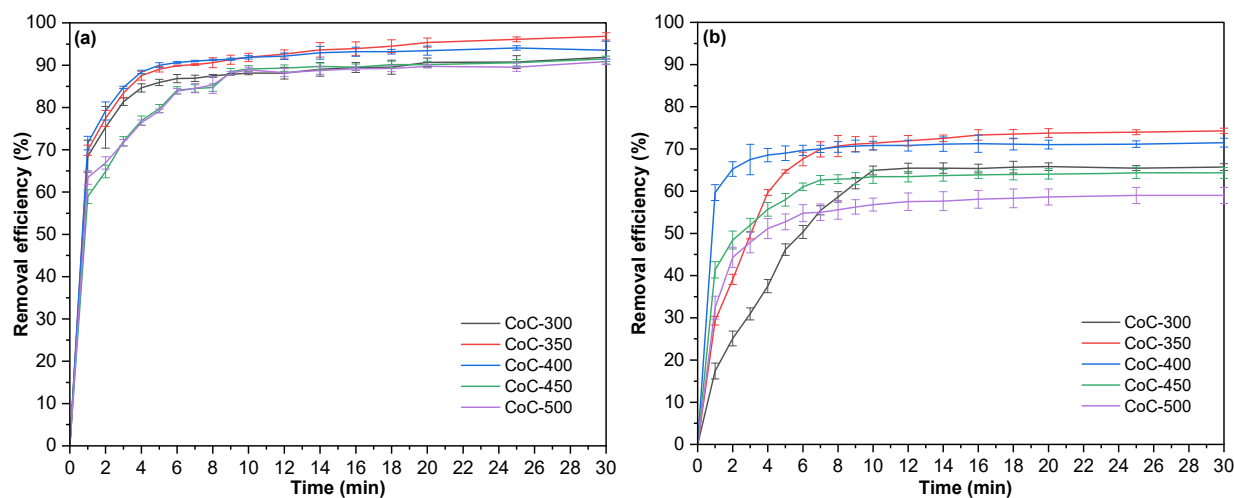


Fig 7. Effect of calcination temperatures of CoC-n on the (a) 25 and (b) 75 mg/L RhB

Table 2. Degradation of RhB by different biochar-supported catalyst

Preparation method	Catalyst	RhB	PMS	Degradation	ROS	Ref.
Solvothermal calcination method	CoC-n (0.3 g/L)	25 mg/L	0.20 g/L	>92.00% in 30 min	$^1\text{O}_2$ , $\text{SO}_4^{\cdot-}$ , and $\cdot\text{OH}$	This work
Sol-gel pyrolysis method	$\text{CoFe}_2\text{O}_4$ doped-biochar (0.1 g/L)	20 mg/L	1.00 mmol/L	100% in 30 min	$\text{O}_2^{\cdot-}$ , $\text{SO}_4^{\cdot-}$ , $\cdot\text{OH}$ , and $^1\text{O}_2$	[41]
Co-pyrolysis and impregnation methods	$\text{Co}_3\text{O}_4$ /RMBC (0.2 g/L)	10 mg/L	0.09 mmol/L	99.70% in 30 min	$^1\text{O}_2$ , $\text{SO}_4^{\cdot-}$ , and $\cdot\text{OH}$	[42]
Hydrothermal pyrolysis method	Fe-doped biochar (0.6 g/L)	50 mg/L	0.60 g/L	97.27% in 10 min	$\text{O}_2^{\cdot-}$ , $\text{SO}_4^{\cdot-}$ , $\cdot\text{OH}$ , and $^1\text{O}_2$	[18]

including  $^1\text{O}_2$ ,  $\text{SO}_4^{\cdot-}$ , and  $\cdot\text{OH}$  radicals, as discussed in Fig. 8. This broad ROS significantly enhances its oxidative potential, enabling effective degradation of a wider array of organic pollutants.

### Mechanism Study in Catalytic PMS Activation

To determine ROS that form, several radical quenching experiments were performed using selective quenching agents, namely ethanol (EtOH), tert-butyl alcohol (TBA), and furfuryl alcohol (FFA), as shown in Fig. 8. CoC-350 was selected as the representative sample for this mechanism study. TBA was employed to selectively quench  $\text{OH}^{\cdot}$ , as it exhibits a high affinity for this species. The reaction rate constant between TBA and  $\text{OH}^{\cdot}$  was determined to be within the range of  $3.8\text{--}7.6 \times 10^8 \text{ M}^{-1} \text{ s}^{-1}$ . Both  $\text{OH}^{\cdot}$  and  $\text{SO}_4^{\cdot-}$  were quenched with EtOH, with reaction rate constants of  $9.1 \times 10^6$  and  $3.5 \times 10^7 \text{ M}^{-1} \text{ s}^{-1}$ , respectively [43]. FFA was utilized as a quenching agent for both  $^1\text{O}_2$  and  $\text{OH}^{\cdot}$ , displaying rate constants of  $1.2 \times 10^8$  and  $1.5 \times 10^{10} \text{ M}^{-1} \text{ s}^{-1}$ , respectively [8,44].

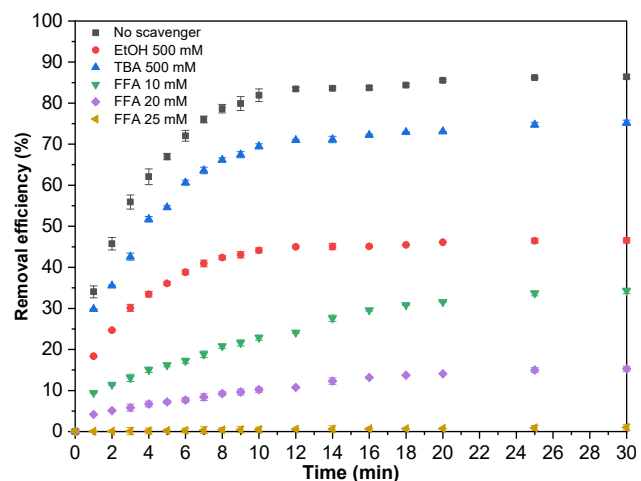


Fig 8. Influence of radical scavengers on RhB degradation in CoC-350/PMS system

The results of the treatment process showed that the addition of 500 mM EtOH dramatically reduced the RhB degradation efficiency from 86.00 to 46.00%. The effectiveness of RhB degradation was, however, less inhibited by TBA. Therefore,  $\text{SO}_4^{\cdot-}$ , a free radical produced

in the CoC/PMS system, may play a key role in RhB degradation. The presence of FFA at concentrations of 10 and 20 mM strongly reduced RhB degradation to 34.00 and 15.00%, respectively, while the FFA concentration of 25 mM almost completely inhibited the RhB degradation, proving that  $^1\text{O}_2$  was formed in the CoC/PMS system and its critical role in RhB degradation. These findings showed that RhB degradation was caused by  $\cdot\text{OH}$ ,  $\text{SO}_4^{\cdot-}$  and  $^1\text{O}_2$ , with  $\text{SO}_4^{\cdot-}$  and  $^1\text{O}_2$  playing the most significant roles.

## ■ CONCLUSION

In conclusion, CoC-n biochar composites, derived from durian shells and doped with cobalt, were successfully synthesized using a simple and green approach – hydrothermal pretreatment, metal doping via solvothermal treatment, and calcination. These composites exhibited effective capability in activating PMS for the efficient degradation of RhB dye. The catalytic performance of the composites was significantly improved, resulting in a fivefold increase in RhB degradation compared to using PMS alone and a tenfold increase compared to using the catalyst alone, all within a 30-min treatment duration. The degradation efficiency reached as high as 92.00 and 74.30% for RhB concentration of 25 and 75 mg/L. Quenching experiments demonstrated the involvement of  $\text{SO}_4^{\cdot-}$ ,  $\text{OH}\cdot$ , and  $^1\text{O}_2$  in the degradation of RhB. These materials hold great potential for the treatment of dye-contaminated wastewater, offering cost-effective and high-performance catalysts derived from biomass sources.

## ■ ACKNOWLEDGMENTS

We acknowledge the support from HUTECH University and the Institute for Tropical Technology and Environment Protection for this study.

## ■ CONFLICT OF INTEREST

The authors declare no potential conflicts of interest concerning this article's research, authorship, and/or publication.

## ■ AUTHOR CONTRIBUTIONS

Anh Mai Hoang Trinh and Thinh Phu Le conducted the experiment and formal analysis and wrote the manuscript draft; Khoi Anh Tran did the concept of

methodology; Nga Hoang Nguyen Do, and Viet Tan Tran wrote and revised the manuscript; Kien Anh Le provided the resources; and Phung Kim Le checked the data accuracy and revised the manuscript. All authors agreed to the final version of this manuscript.

## ■ REFERENCES

- [1] Chandanshive, V., Kadam, S., Rane, N., Jeon, B.H., Jadhav, J., and Govindwar, S., 2020, *In situ* textile wastewater treatment in high rate transpiration system furrows planted with aquatic macrophytes and floating phytobeds, *Chemosphere*, 252, 126513.
- [2] Jain, R., Mathur, M., Sikarwar, S., and Mittal, A., 2007, Removal of the hazardous dye rhodamine B through photocatalytic and adsorption treatments, *J. Environ. Manage.*, 85 (4), 956–964.
- [3] Bello, O.S., Alabi, E.O., Adegoke, K.A., Adegboyega, S.A., Inyinbor, A.A., and Dada, A.O., 2020, Rhodamine B dye sequestration using *Gmelina aborea* leaf powder, *Heliyon*, 6 (1), e02872.
- [4] Wang, M., Wang, F., Wang, P., Chu, H., Fu, H., Zhao, C., Wang, C.C., and Zhao, Y., 2023, Highly efficient and selective organic pollutants degradation via peroxymonosulfate activation over micron-sized Co-MOF: Nearly 100% singlet oxygen mechanism, *Sep. Purif. Technol.*, 326, 124806.
- [5] Kohantorabi, M., Moussavi, G., and Giannakis, S., 2021, A review of the innovations in metal- and carbon-based catalysts explored for heterogeneous peroxymonosulfate (PMS) activation, with focus on radical vs. non-radical degradation pathways of organic contaminants, *Chem. Eng. J.*, 411, 127957.
- [6] Dai, Z., Li, D., Ao, Z., Wang, S., and An, T., 2021, Theoretical exploration of VOCs removal mechanism by carbon nanotubes through persulfate-based advanced oxidation processes: Adsorption and catalytic oxidation, *J. Hazard. Mater.*, 405, 124684.
- [7] Ma, Y., Ji, B., Lv, X., Xiong, D., Zhao, X., Xie, H., and Zhang, Z., 2022, Confined heterogeneous catalysis by boron nitride- $\text{Co}_3\text{O}_4$  nanosheet cluster for peroxymonosulfate oxidation toward ranitidine removal, *Chem. Eng. J.*, 435, 135126.

- [8] Gao, L., Guo, Y., Zhan, J., Yu, G., and Wang, Y., 2022, Assessment of the validity of the quenching method for evaluating the role of reactive species in pollutant abatement during the persulfate-based process, *Water Res.*, 221, 118730.
- [9] Xu, M., Li, J., Yan, Y., Zhao, X., Yan, J., Zhang, Y., Lai, B., Chen, X., and Song, L., 2019, Catalytic degradation of sulfamethoxazole through peroxymonosulfate activated with expanded graphite loaded  $\text{CoFe}_2\text{O}_4$  particles, *Chem. Eng. J.*, 369, 403–413.
- [10] Zeng, H., Zhang, W., Deng, L., Luo, J., Zhou, S., Liu, X., Pei, Y., Shi, Z., and Crittenden, J., 2018, Degradation of dyes by peroxymonosulfate activated by ternary  $\text{CoFeNi}$ -layered double hydroxide: Catalytic performance, mechanism and kinetic modeling, *J. Colloid Interface Sci.*, 515, 92–100.
- [11] Wu, Y., Mao, S., Liu, C., Pei, F., Wang, F., Hao, Q., Xia, M., and Lei, W., 2022, Enhanced degradation of chloramphenicol through peroxymonosulfate and visible light over Z-scheme photocatalysts: Synergetic performance and mechanism insights, *J. Colloid Interface Sci.*, 608, 322–333.
- [12] Guo, H., Zhou, X., Zhang, Y., Yao, Q., Qian, Y., Chu, H., and Chen, J., 2020, Carbamazepine degradation by heterogeneous activation of peroxymonosulfate with lanthanum cobaltite perovskite: Performance, mechanism and toxicity, *J. Environ. Sci.*, 91, 10–21.
- [13] Banerjee, P., and Bhattacharya, P., 2021, Investigating cobalt in soil-plant-animal-human system: Dynamics, impact and management, *J. Soil Sci. Plant Nutr.*, 21 (3), 2339–2354.
- [14] Xu, H., Jiang, N., Wang, D., Wang, L., Song, Y., Chen, Z., Ma, J., and Zhang, T., 2020, Improving PMS oxidation of organic pollutants by single cobalt atom catalyst through hybrid radical and non-radical pathways, *Appl. Catal., B*, 263, 118350.
- [15] Mian, M.M., and Liu, G., 2020, Activation of peroxymonosulfate by chemically modified sludge biochar for the removal of organic pollutants: Understanding the role of active sites and mechanism, *Chem. Eng. J.*, 392, 123681.
- [16] Tkachenko, V., Marzban, N., Vogl, S., Filonenko, S., and Antonietti, M., 2023, Chemical insights into the base-tuned hydrothermal treatment of side stream biomasses, *Sustainable Energy Fuels*, 7 (3), 769–777.
- [17] Jiang, T., Wang, B., Gao, B., Cheng, N., Feng, Q., Chen, M., and Wang, S., 2023, Degradation of organic pollutants from water by biochar-assisted advanced oxidation processes: Mechanisms and applications, *J. Hazard. Mater.*, 442, 130075.
- [18] Zang, T., Wang, H., Liu, Y., Dai, L., Zhou, S., and Ai, S., 2020, Fe-doped biochar derived from waste sludge for degradation of rhodamine B via enhancing activation of peroxymonosulfate, *Chemosphere*, 261, 127616.
- [19] Liu, J., Jiang, J., Wang, M., Kang, J., Zhang, J., Liu, S., Tang, Y., and Li, S., 2022, Peroxymonosulfate activation by cobalt particles embedded into biochar for levofloxacin degradation: Efficiency, stability, and mechanism, *Sep. Purif. Technol.*, 294, 121082.
- [20] Wang, S., and Wang, J., 2023, Bimetallic and nitrogen co-doped biochar for peroxymonosulfate (PMS) activation to degrade emerging contaminants, *Sep. Purif. Technol.*, 307, 122807.
- [21] FAO, 2023, *Durian Global Trade Overview 2023*, Food and Agriculture Organization of the United Nations, Rome, Italy.
- [22] Ly, T.B., Pham, C.D., Le, K.A., and Le, P.K., 2023, Novel production methods of biochar from durian (*Durio zibethinus*) rind to be used as smokeless fuel, *Chem. Eng. Trans.*, 106, 337–342.
- [23] Nguyen, T.H., Nguyen, X.H., Do, T.G., and Nguyen, L.H., 2023, Development of biochar supported  $\text{NiFe}_2\text{O}_4$  composite for peroxydisulfate (PDS) activation to effectively remove moxifloxacin from wastewater, *Chem. Eng. J. Adv.*, 16, 100550.
- [24] Thuong, N.T., Nhi, N.T.T., Nhung, V.T.C., Bich, H.N., Quynh, B.T.P., Bach, L.G., and Trinh, N.D., 2019, A fixed-bed column study for removal of organic dyes from aqueous solution by pre-treated durian peel waste, *Indones. J. Chem.*, 19 (2), 486–494.

- [25] Panakkal, E.J., Cheenkachorn, K., Gundupalli, M.P., Kitiborwornkul, N., and Sriariyanun, M., 2021, Impact of sulfuric acid pretreatment of durian peel on the production of fermentable sugar and ethanol, *J. Indian Chem. Soc.*, 98 (12), 100264.
- [26] Ge, J., Wu, Y., Han, Y., Qin, C., Nie, S., Liu, S., Wang, S., and Yao, S., 2020, Effect of hydrothermal pretreatment on the demineralization and thermal degradation behavior of eucalyptus, *Bioresour. Technol.*, 307, 123246.
- [27] Archanjo, B.S., Mendoza, M.E., Albu, M., Mitchell, D.R.G., Hagemann, N., Mayrhofer, C., Mai, T.L.A., Weng, Z., Kappler, A., Behrens, S., Munroe, P., Achete, C.A., Donne, S., Araujo, J.R., van Zwieten, L., Horvat, J., Enders, A., and Joseph, S., 2017, Nanoscale analyses of the surface structure and composition of biochars extracted from field trials or after co-composting using advanced analytical electron microscopy, *Geoderma*, 294, 70–79.
- [28] Hu, P., Su, H., Chen, Z., Yu, C., Li, Q., Zhou, B., Alvarez, P.J.J., and Long, M., 2017, Selective degradation of organic pollutants using an efficient metal-free catalyst derived from carbonized polypyrrole via peroxymonosulfate activation, *Environ. Sci. Technol.*, 51 (19), 11288–11296.
- [29] Liu, X., and Prewitt, C.T., 1990, High-temperature X-ray diffraction study of  $\text{Co}_3\text{O}_4$ : Transition from normal to disordered spinel, *Phys. Chem. Miner.*, 17 (2), 168–172.
- [30] Sasaki, S., Fujino, K., and Takéuchi, Y., 1979, X-ray determination of electron-density distributions in oxides, MgO, MnO, CoO, and NiO, and atomic scattering factors of their constituent atoms, *Proc. Jpn. Acad., Ser. B*, 55 (2), 43–48.
- [31] Li, C., Chen, T., Xu, W., Lou, X., Pan, L., Chen, Q., and Hu, B., 2015, Mesoporous nanostructured  $\text{Co}_3\text{O}_4$  derived from MOF template: A high-performance anode material for lithium-ion batteries, *J. Mater. Chem. A*, 3 (10), 5585–5591.
- [32] Xu, J., Gao, P., and Zhao, T.S., 2012, Non-precious  $\text{Co}_3\text{O}_4$  nano-rod electrocatalyst for oxygen reduction reaction in anion-exchange membrane fuel cells, *Energy Environ. Sci.*, 5 (1), 5333–5339.
- [33] Tian, R., Dong, H., Chen, J., Li, R., and Xie, Q., 2020, Amorphous  $\text{Co}_3\text{O}_4$  nanoparticles-decorated biochar as an efficient activator of peroxymonosulfate for the removal of sulfamethazine in aqueous solution, *Sep. Purif. Technol.*, 250, 117246.
- [34] Zou, Y., Li, W., Yang, L., Xiao, F., An, G., Wang, Y., and Wang, D., 2019, Activation of peroxymonosulfate by  $\text{sp}^2$ -hybridized microalgae-derived carbon for ciprofloxacin degradation: Importance of pyrolysis temperature, *Chem. Eng. J.*, 370, 1286–1297.
- [35] Tan, L.N., Nguyen, N.C.T., Trinh, A.M.H., Do, N.H.N., Le, K.A., and Le, P.K., 2023, Eco-friendly synthesis of durable aerogel composites from chitosan and pineapple leaf-based cellulose for Cr(VI) removal, *Sep. Purif. Technol.*, 304, 122415.
- [36] Penjumras, P., Abdul Rahman, R.B., Talib, R.A., and Abdan, K., 2014, Extraction and characterization of cellulose from durian rind, *Agric. Agric. Sci. Procedia*, 2, 237–243.
- [37] Xue, M., Xu, H., Tan, Y., Chen, C., Li, B., and Zhang, C., 2021, A novel hierarchical porous carbon derived from durian shell as enhanced sulfur carrier for high performance Li-S batteries, *J. Electroanal. Chem.*, 893, 115306.
- [38] Yang, Q., Zhang, Y., Liang, J., Luo, Y., Liu, Q., Yang, Y., and Sun, X., 2022, Facile hydrothermal synthesis of co-glycerate as an efficient peroxymonosulfate activator for rhodamine B degradation, *Colloids Surf., A*, 648, 129239.
- [39] Nethravathi, C., Sen, S., Ravishankar, N., Rajamathi, M., Pietzonka, C., and Harbrecht, B., 2005, Ferrimagnetic nanogranular  $\text{Co}_3\text{O}_4$  through solvothermal decomposition of colloiddally dispersed monolayers of  $\alpha$ -cobalt hydroxide, *J. Phys. Chem. B*, 109 (23), 11468–11472.
- [40] Xu, Z.P., and Zeng, H.C., 1998, Thermal evolution of cobalt hydroxides: a comparative study of their various structural phases, *J. Mater. Chem.*, 8 (11), 2499–2506.
- [41] Pan, Y., Meng, F., Bai, J., Song, B., and Cao, Q., 2024, Highly efficient peroxymonosulfate activation by  $\text{CoFe}_2\text{O}_4$ @attapulgit-biochar

- composites: Degradation properties and mechanism insights, *J. Environ. Chem. Eng.*, 12 (3), 112579.
- [42] Sun, X., Wang, X., Xu, D., and Dai, P., 2023,  $\text{Co}_3\text{O}_4$  decoration on iron-contained biochar composite fabricated by co-pyrolysis of red mud and spent coffee ground: A synergistic hybrid for Rhodamine B degradation via peroxymonosulfate activation, *J. Environ. Chem. Eng.*, 11 (5), 110706.
- [43] Zeng, T., Zhang, X., Wang, S., Niu, H., and Cai, Y., 2015, Spatial confinement of a  $\text{Co}_3\text{O}_4$  catalyst in hollow metal–organic frameworks as a nanoreactor for improved degradation of organic pollutants, *Environ. Sci. Technol.*, 49 (4), 2350–2357.
- [44] Tian, Z., Chen, Q., Ren, S., Zhang, H., Tian, W., Sun, H., and Wang, S., 2023, Effects of cobalt salts on biomass conversion to functional carbon-based catalysts for peroxymonosulfate activation, *Chem. Eng. J.*, 469, 143856.